



Original

## Failure analysis of stainless steel lanyard wire rope

A. Sambasiva Rao

A. K. Singh\*

*Defence Metallurgical Research Laboratory, Kanchanbagh, Hyderabad, 5000258, India*

---

**Abstract:** Present work describes the failure analysis of AISI 304 stainless steel consisting of 7x19 construction lanyard wire rope which has failed during service. The microstructures and properties of failed wire rope have been investigated and compared with unused wire rope. Both the periphery and fracture surface of the wire rope display the presence of corrosion debris enriched with O and Cl. The fracture surfaces of the failed and unused wire ropes display intergranular and dimples, respectively. The lanyard wire rope has been exposed in corrosive atmosphere and failed in intergranular mode due to enrichment of O and Cl along the grain boundaries.

*Keywords:* Lanyard wire rope; Stainless steel; EPMA; Intergranular corrosion

---

### 1. INTRODUCTION

Lanyard wire ropes or cable assemblies are cables which are comprised of many spiralled bundles of wire. In general, lanyard terminus ends are equipped with connectors which make it possible to attach them to other fall protection system (Baszczynski, 2007). This covers a very broad range of wire rope products, and wire rope lanyards can be extensively customized to meet the needs of a multitude of applications. These are commonly used in security, holding, hanging, attaching, anchoring, lifting, supporting and pulling. The wire ropes have been designed for specific purpose depending on a particular application (Costello, 1990).

Wire rope consists of multiple strands of wire filament which themselves are twisted together before being wound

helically around a core. The number of each set of strands depends on the strength requirements for proposed application (Chaplin, 1995). The construction of lanyard wire rope is defined as  $n \times p$  where  $n$  and  $p$  are number of strands and number of wires in each strand, respectively (Costello, 1990). A common lanyard wire rope is represented by as 7x19 construction which suggests that this is made up of nineteen small wires being twisted together with seven other similar bundles (Davis, 1979).

Among all other materials, stainless steel lanyard is usually found in very unique work areas. Apart from the other features, high strength, excellent abrasion resistance and corrosion resistance are the most important characteristics (Baszczynski, 2007). Stainless steels are used in corrosive environment particularly in area of petrochemical industries and humid atmosphere (Parrott & Pitts, 2011). These wires are also coated with different plastic materials to enhance both the functional as well as appearance. The major defects in wire ropes are by and large introduced failed due to oxidation, corrosion,

\* Corresponding author.

E-mail address: [singh\\_ashok3@rediffmail.com](mailto:singh_ashok3@rediffmail.com) (A. K. Singh).

excessive heat, chemical degradation etc. In addition, environmental condition particularly humid atmosphere containing sea water also initiates the degradation of wire ropes. It is to be noted that the sea water contains chlorine that corrodes the metals in general and stainless steel in particular (Brown, 1977; Parrott & Pitts, 2011).

The present work is thus concerned with the failure analysis of a 7×19 construction lanyard wire rope which has failed during application in wet and humid environment. Wire rope is made up of 7 strands and each strand comprises 19 wires (rope length: 3 feet 6 inches). The microstructure and properties of unused wire has also been investigated and compared with the failed rope.

## 2. EXPERIMENTAL PROCEDURE

Initially, visual examinations of the broken lanyard wire rope were carried out and the photographs of the failed wire rope were captured using digital camera. The analyzed chemical composition of the failed wire rope is given in Table 1. It suggests that the material used for wire rope is austenitic stainless steel and conforms to AISI 304 grade. Wires were cut from the failed wire rope near the actual fractures and prepared for metallographic examination. The polished surface was etched with aquaregia (50% HCl and 50% HNO<sub>3</sub> by volume). Microstructural characterization was done using optical microscope. The failed wires at the fractured surface were separated from the long wire rope and then bound together with a copper wire. These wires were cleaned ultrasonically in acetone to remove any dirt and other lubricant residues over the fracture surface. The fracture surfaces of the multiple wire failed sections near actual fracture were examined under a Field Electron and Ion (FEI) make environmental scanning electron microscope (Model: Quanta 400) to evaluate the contaminated products over the fracture surface as well as mode of fracture.

As received failed rope wires were further examined using Electron Probe Micro Analyser (EPMA) to study the grain boundary constituents that have caused the degradation of microstructure. Samples were prepared as per metallographic examination and analysed in un-etched condition for EPMA examination. Back scattered electron (BSE) image, elemental distribution mapping and line profile for different elements were analyzed using CAMECA make, SX-100 model EPMA. Quantitative

Quantitative analysis was carried out with an operating voltage of 20 kV and with a stabilized beam current of 20 nA. A LiF (Lithium Fluoride) crystal was employed to diffracting Mn K $\alpha$  and Ni K $\alpha$ ; PET (Pentaerythritol) crystal was used for diffracting Cr K $\alpha$  and Cl K $\alpha$  and TAP (Thallium Acid Phthalate) crystal was employed for diffracting Si K $\alpha$  X-ray lines. Pseudocrystals of PC2 having 2d value of 98 Å was utilized for Oxygen analysis. X-ray intensities were obtained both on respective pure metallic standards and also on samples with identical operating conditions. Absolute elemental concentrations were attained using built in analytical software with essential Atomic number (Z), Absorption and Fluorescence (ZAF) correction to get accurate weight/atom percentage of constituents in the respective sample.

Wire rope strands were separated from the rope and cut to desired length for tensile testing. Tensile properties of failed, used (but not failed) and unused wire ropes were evaluated to know the maximum load bearing capacity. Room temperature tensile tests were conducted with a strand containing 19 wires on screw driven Instron (5500 R) testing machine (Instron Corporation, Norwood, MA). Three specimens were tested in each wire rope and average values are reported in Table 2. Fracture surfaces of tensile specimens were again examined under environmental scanning electron microscope (SEM: FEI Quanta 400).

## 3. RESULTS AND DISCUSSION

The broken wire rope in as-received condition is shown in Figure 1(a-c). This displays dark brownish colour. The wire rope supplied with two broken ends (Figure 1a). This consists of many small diameter wires wound together into strands and then these strands are knit jointly into a wire rope. The end fittings of the wire rope are fastened with open swaged socket. Broken end region displays several wires unwound and loosen from their strands (Figure 1b and c). Chemical composition of the wire rope indicates that the wires are made using austenitic stainless steel AISI 304 grade (Table 1).

Optical microstructures of failed wire rope are shown in Figure 2. This displays the presence of typical equiaxed austenitic grains along with annealing twins (Figure 2a). The average grain size is ~ 15  $\mu$ m (ASTM No. 8.5). The grain size near and away from failed region appears to be same. The optical microstructure of the wire exhibits two

features namely (a) overall grain size is nearly uniform from center to periphery and (b) several cracks along the grain boundaries at the periphery of the wire rope (Figure 2b and c). Presence of annealing twins within the equiaxed austenitic grains indicates that the wire rope is used in annealed condition (Figure 1, 2a). This also suggests that the rope wires are initially prepared by wire drawing and subsequently annealed. In addition, several grains have been dislodged from periphery of the individual broken wire (Figure 2b and c). The dislodged materials have broken and separated from the wire along the grain boundaries. This clearly reveals that the grain boundaries have significantly weakened during service. Very close to the fractured area, the microstructure exhibits extensive material degradation due to grain boundary weakening.

BSE micrograph close to the fracture obtained in un-etched condition exhibits continuous thin film along grain boundaries (Figure 3). This observation is analogue to the optical microstructure (Figure 2). The X-ray elemental mappings of Cr, O, Cl, Ni and Mn elements of failed wire rope in un-etched condition obtained by EPMA are shown in Figure 4. Elemental distribution mapping reveals that the grain boundaries are enriched with Oxygen, Chlorine and Chromium. On the other hand, uniform distributions of Nickel and Manganese are observed in the matrix.

In order to confirm the results of elemental mapping, X-ray line scan technique has been employed for Oxygen Chlorine and Chromium elements and results are shown in Figure 5. This reflects evidently that the line scan profiles have validated the enrichment of Oxygen, and Chlorine at the grain boundary. Line profile has also displayed the chromium enrichment at the grain boundary as well as the depletion at either side of the grain (i.e. vicinity of grain boundary). The weakening of grain boundaries along with dislodged materials from the periphery of the wire therefore indicates that the rope is exposed to corrosive environment during the service. Presence of Cl and O at the grain boundaries in the form of thin film supports the same.

The fracture surfaces of failed wire rope near the actual fractures are shown in Figure 6 (a-d). Thick layer of foreign material deposition is exhibited over the fracture surface of the individual wires and also all around the surface of each wire. In fact fracture surfaces of the failed rope have shown the presence of corrosion debris which has masked the actual fracture (Figure 6). The fracture surfaces of the wire appear to be rough and the individual

wire does not show distinctive mode of fracture features. These are similar to mud cracks with oxide layer (Figure 6b-d). The Energy Dispersive Spectroscopy (EDS) spectrum taken on fracture surface of the failed rope near the actual fractures has revealed the presence of chlorine and oxygen in addition to matrix elements (Figure 7). These results are well agreement with those obtained by EPMA analysis (Figure 4 and 5). All the wires in the failed rope have shown similar behaviour.

Tensile properties of failed, used (but not failed) and unused wire ropes are summarized in Table 2. Fascinatingly, the load bearing capacity of the failed wire has reduced to nearly 1/4 of the unused wire rope (Table 2). The used (but not failed) wire on the other hand also displays reduction in breaking load nearly 1/2 times than the unused wire rope. The ultimate tensile strength values of the wires reported in Table 2 also support the same. This also reflects that the properties of the rope have deteriorated significantly during service.

The results of the tensile tests of the failed and unused wires have been utilized to explain the occurrence of typical fracture features of the failed wire rope. The fracture surfaces of tensile tested specimens of the failed and unused wires are shown in Figure 8 and 9. The flat fracture with no reduction in the cross sectional area is seen in the failed individual wire (Figure 8a). The fracture surface of the wire appears to be rough and clearly reveal the presence of intergranular fracture (Figure 8c-d). The failed wire clearly shows typical brittle fracture in spite of the presence of corrosive debris. Fracture surface of tensile tested wire of the failed rope displayed a thick metallic layer covered around the circumference of the failed wire.

Table 1. Chemical composition of the failed wire rope.

Element	C	S	Ni	Cr	Mn	Si	Fe
Wt.%	0.08	0.002	8.2	19.7	1.8	0.92	Balance

Table 2. Tensile properties of the strands for unused, used (not failed) and failed wire ropes.

Sl.No.	Description	Max. Tensile Breaking Load (kN)	UTS (MPa)
	Strand from Unused Wire Rope	3.00	1490
	Strand from used (not failed) Wire Rope	1.35	685
	Strand from Failed Wire Rope	0.70	378

However, a part of the thick layer of the individual wire has fallen away from close to tensile fracture during tensile deformation (Figure 8a).

Tensile tested fracture surfaces of the unused wires display entirely different features (Figure 9) than that of the failed wires in terms of mode of failure (Figure 8). The fracture surface of unused wire rope exhibits smooth surface finish around the rope outer surface (Figure 9a). The fracture features displays sufficient necking indicating typical ductile mode of failure (Figure 9b).

Unused wire rope has undergone significant necking before tensile failure and finally failed in ductile mode. This clearly suggests that the failed wire rope has slowly deteriorated during service and then suddenly failed with intergranular fracture mode. It appears that the crack propagated along the weak grain boundaries and finally failed in brittle mode of fracture (Figure 8).

When passive metals such as the stainless steels corrode, the corrosion develops where passivity has been destroyed. If there are halogenides such as chlorides present in the environment, these can interact with passive film locally and break it by introducing small isolated spots (Bensalah, 2012; Leffler, 1998). This is also termed as pitting corrosion. This type of corrosion is likely due to chlorine-induced pitting of the stainless steel material from the chloride containing humid environment. The chlorides can then react with chromium to form soluble chromium chloride ( $\text{CrCl}_3$ ) following  $2\text{Cr} + 3\text{Cl}_2 = 2\text{CrCl}_3$  reaction. As a result, Cr at the grain boundaries is partly dissolved leaving only the corrosion prone iron (Tverberg, 2001). This also introduces depletion of Cr in neighboring area of the grain boundaries which are prone to fail in intergranular mode (Figure 5 and 8).

The occurrence of intergranular corrosion has also been reported even without the chromium carbide precipitates at the grain boundaries (Kodgire & Kodgire, 2013). This has been attributed to high energy associated with the grain boundaries which are preferentially corroded (become anode) due to their low electrode potential in comparison to grain interior. The present lanyard rope has also failed in intergranular mode due to the formation of  $\text{CrCl}_3$  in presence of humid environment.

As mentioned above, microstructure of the failed wire rope exhibits thin film at the grain boundaries consisting of O and Cl. It appears that the presence of both the high O and Cl at the grain boundaries can be due to corrosive atmosphere. The chlorine ions from the water

content / vapours from humid atmosphere have initially reacted with chromium oxide passive film formed on the surface of the wire and then diffused within the material along the grain boundaries. The depletion of the Cr in vicinity of the grain boundaries supports the same (Figure 5). This has resulted in the failure of the wire rope in intergranular mode due to substantial weakening of grain boundaries.

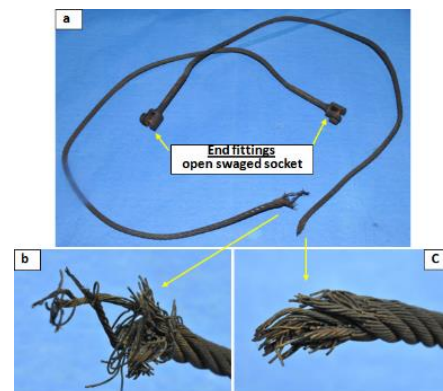


Fig. 1. Photograph of failed wire rope: (a) as-received condition, (b) one end of the broken rope, (c) another end of the broken rope displays several wires unwound from its strands and loosens from their strands.

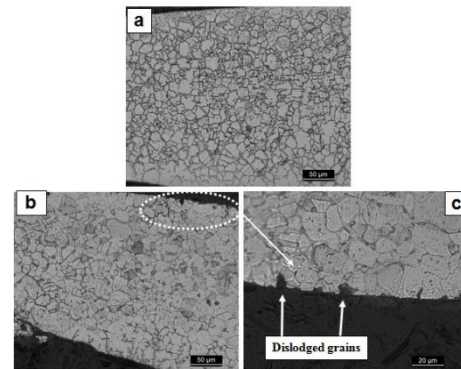


Fig. 2. Optical micrograph of failed wire rope shows (a) austenitic grain structure with annealing twins, (b) few grains are dislodged from the grain boundaries at the surface near fracture and (c) high magnification of dislodged grains.

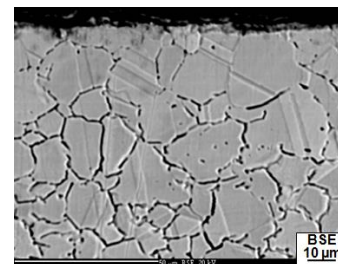


Fig. 3. EPMA-BSE microstructure of the individual wire near failed end showing dark network along grain boundaries.

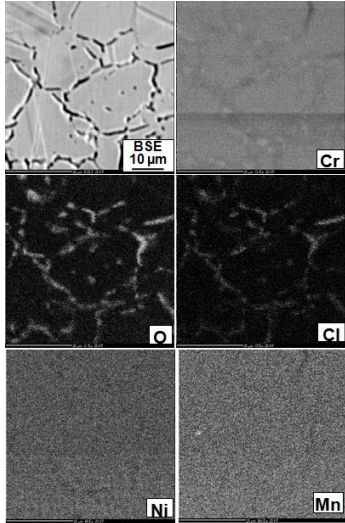


Fig. 4. X-ray elemental distribution mappings of Cr, O, Cl Ni and Mn obtained by EPMA illustrates enrichment of Cr, Cl and O along the grain boundary.

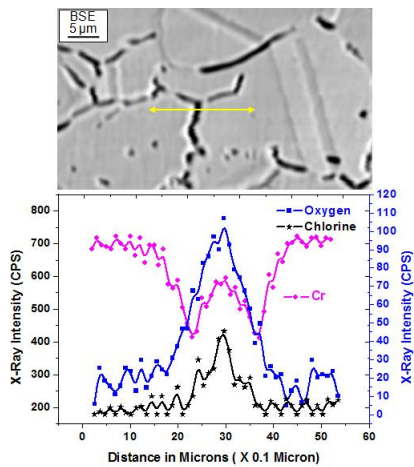


Fig. 5. EPMA Line profile of the elements O, Cl and Cr across the grain boundary demonstrates as reflected in the X-ray mappings.

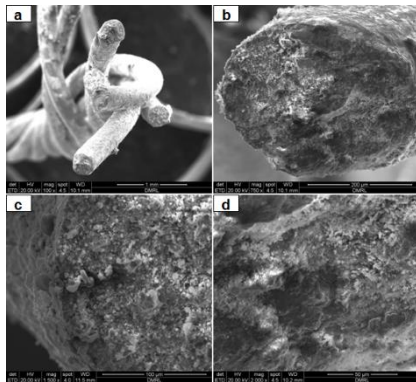


Fig. 6. SEM fractographs of individual failed wire obtained at (a) Low magnification and (b-d) high magnification show thick layer deposition of corrosion debris over the fracture surface.

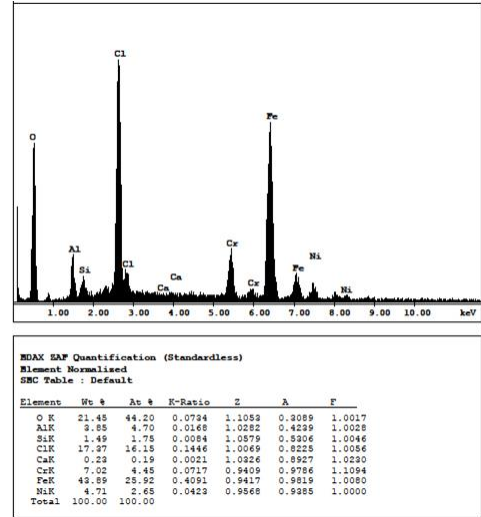


Fig. 7. EDS Spectrum taken from the fracture surface of the failed individual wire exhibits presence of O and Cl in addition to matrix elements.

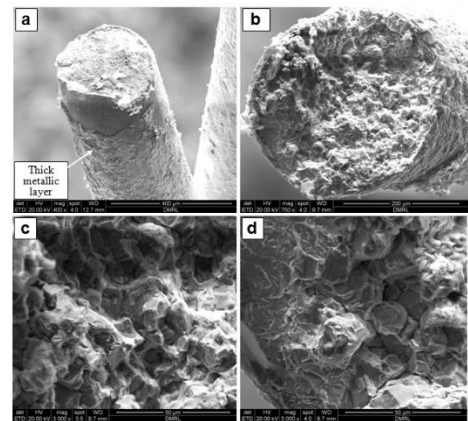


Fig. 8. SEM fractographs of tensile tested failed wire rope: (a) low magnification and (b-d) High magnification reveals flat fracture with intergranular mode of failure.

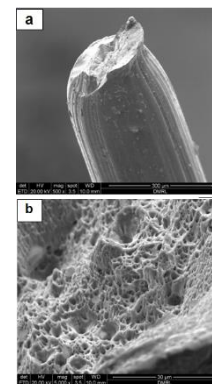


Fig. 9. SEM fractographs of tensile tested unused wire rope: (a) low magnification (b) high magnification showing considerable reduction in size with dimple mode of fracture.

#### 4. CONCLUSIONS

The failed wire rope near the actual fracture region consists of large amount of oxygen and chlorine present in the initiation sites for cracks in the material.

The load bearing capacity of the failed wire rope strand has significantly reduced to nearly 1/4 times to that of the new unused wire rope in identical testing conditions.

Fracture surfaces of tensile tested failed and unused lanyard rope individual wires have shown intergranular and ductile dimple modes of fracture, respectively.

The lanyard wire rope has been exposed in corrosive atmosphere and failed in intergranular mode due to enrichment of O and Cl along the grain boundaries.

#### ACKNOWLEDGEMENTS

The authors wish to acknowledge Defence Research and Development Organization for financial support. Authors are grateful to Dr Vikas Kumar, Director, Defence Metallurgical Research Laboratory for his kind encouragement. Authors thank Electron Microscopy, Structure and Failure Analysis and Mechanical Behaviour Groups of DMRL for their kind help.

#### CONFLICT OF INTEREST

The authors have no conflicts of interest to declare.

#### REFERENCES

- Baszczyński, K. (2007). Dynamic Strength Tests for Low Elongation Lanyards, *International Journal of Occupational Safety and Ergonomics (JOSE)*, 13(1), 39–48.
- Bensalah, N. (2012). Pitting Corrosion. *Pitting Corrosion, Corrosive Effects of Chlorides on Metals*, Fong-Yuan Ma, (Chapter 7).
- Brown, B. F. (1977). Stress Corrosion Cracking Control Measures, *National Bureau of Standards Monograph 156*, (Chapter 7).
- Chaplin, C. R. (1995). Failure Mechanisms in Wire Rope. *Engineering Failure Analysis*, 2(1), 45–57.
- Costello, G. A. (1990). *Theory of Wire Rope*. (2 ed.). New York. (Chapter 1).
- Davis, G. J. (1979). Wire Rope Users Manual. *Committee of Wire Rope Producers, American Iron and Steel Institute*, (Chapter 3).
- Kodgire, V. D., & Kodgire, S. V. (2013). *Material Science and Metallurgy for Engineers*. (32 ed.). (Chapter 6).
- Leffler, B. (1998). *Stainless-stainless Steels and their Properties*, (2ed). (Chapter 3).
- Parrott, R., & Pitts, H. (2011). Chloride stress corrosion cracking in austenitic stainless steel. Research Report RR902. *Health and Safety Laboratory, Buxton, UK*.
- Tverberg, J. C. (2001). Stainless Steel in the Brewery, *MBAA TQ*, Technical Quarterly, 38(2), 67–82.